Deep Convection over Africa: Annual Cycle, ENSO, and Trends in the Hotspots

NEIL C. G. HART AND RICHARD WASHINGTON

School of Geography and the Environment, University of Oxford, Oxford, United Kingdom

ROSS I. MAIDMENT

Department of Meteorology, University of Reading, Reading, United Kingdom

(Manuscript received 9 April 2019, in final form 26 September 2019)

ABSTRACT

Africa is one of the three key regions of deep convection in the global tropics. There is a wealth of information on the intensity, variability, and change of convection and associated rainfall in regions across the continent but almost all of this literature is regionally focused and confined to specific seasons. This fragmented approach precludes a continent-wide view of deep convection leaving the following key issues unanswered: When is deep convection the most widespread across Africa? Where on the continent is deep convection most active? Where does widespread convection have the most interannual variability? This paper confronts these questions using a satellite-derived integral of deep convection. At the continental scale, March exhibits the most extensive deep convection whereas the West African monsoon during June–July exhibits the least. El Niño generally suppresses pan-African convective activity while La Niña enhances this activity. These pan-African signals are largely determined by regional hotspots: the eastern Congo hosts the most persistent widespread deep convection, southeastern southern Africa displays the highest interannual variability, and regional highlands maintain local convective activity hotspots. Furthermore, pan-African annual mean convective activity has increased ~10% between 1983 and 2015 with increases of >20% recorded in local hotspots. Results in this study provide a climatological baseline for both observational and model-based studies of African climates and offer insights into when African convection has the greatest potential impact on the general circulation.

1. Introduction

Africa has long been known as one of three key regions of deep convection and diabatic heating that drives the global tropical circulation (Webster 1973). A striking characteristic of that deep convection is its almost perfect symmetry around the equator when averaged through the annual cycle such that convection spans 45° of latitude with a peak near 2°S (Waliser and Gautier 1993). This symmetry likely results from the equitable land area on either side of 0° latitude. No other region in the global tropics has comparable symmetry. African convection is also distinct in being influenced on interannual and interdecadal time scales by all three ocean basins.

Through the annual cycle, solar heating and water vapor transport render a broad swath of the atmosphere conducive to deep convection, although in most seasons and regions of Africa not through a recognizable intertropical convergence zone (Nicholson 2018)—the exception being West Africa. The strong seasonality and regional location of the deep tropical convection results in distinctive responses to remote forcing. For example, El Niño events are generally dry in West Africa from July to September (Ward 1992), wet in East Africa from October to December (Ogallo 1988), and dry in southern Africa from January to March (Lindesay 1988).

Denotes content that is immediately available upon publication as open access.

Supplemental information related to this paper is available at the Journals Online website: https://doi.org/10.1175/JCLI-D-19-0274.s1.

Corresponding author: Neil C. G. Hart, neil.hart@ouce.ox.ac.uk

DOI: 10.1175/JCLI-D-19-0274.1

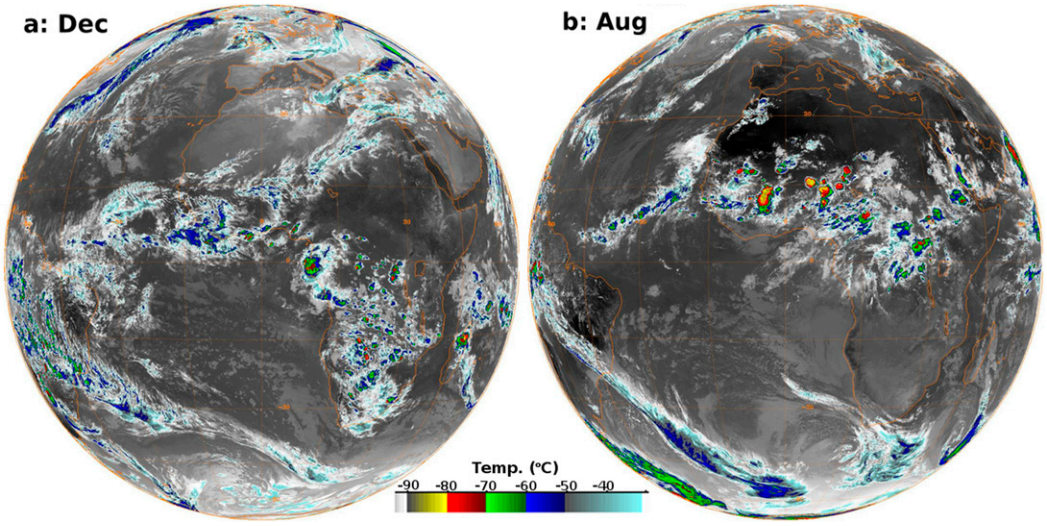

FIG. 1. Typical geostationary satellite imagery of convective outbreaks over Africa during (a) austral summer, taken at 1812 UTC 21 Dec 2017, and (b) boreal summer, taken at 1812 UTC 21 Aug 2017. (Courtesy: NOAA-NCEI Global ISCCP B1 Browse System; Knapp 2008).

The upshot of the strong seasonality, wide latitudinal excursion of tropical convection through the annual cycle, and contrasting influence of remote modes is that the understanding of deep convection in Africa is fragmented into specific regions and seasons. The primary regions are West Africa/Sahel (which dominates the literature), East Africa, southern Africa, and, occasionally, central Africa (which is the region of most widespread convection). What is missing from this fragmented view is an integrated assessment of African deep convection onto which map some rather basic questions such as the following: What is the annual cycle of deep convection for the continent as a whole? Which month features the largest spatial extent of deep convection? Does deep convection dominate on the continent in La Niña or El Niño years and in which months? And is there a trend in deep convection over the satellite era? It is the purpose of this paper to engage with these concerns. The overall objective is to build a regionally integrated picture of Africa-wide deep convection that is long overdue.

These questions can be summed up pictorially in Fig. 1. There is extensive literature covering convection during the austral (Fig. 1a) and boreal (Fig. 1b) summers, but quantitatively which summer represents a more active season for deep convection? And what is the climatological spatial and temporal structure of convection during the transition between these two states?

The advent of convective-permitting climate models run at continental scale (e.g., Stratton et al. 2018), whereby deep convection and its characteristics are beginning to be better represented, is a further impetus for this research. This study provides the observational assessment of the spatiotemporal distribution of widespread convection, which is needed to diagnose the fidelity of these models in simulating the climatology of African convection. A key part of this climatology is the consideration of regional hotspots for deep convection. Frequent outbreaks of organized deep convection in one locale will lead to repeated heating of the atmospheric column with associated adjustments in the regional circulation. As a result, deep convective hotspots may act as ''engine rooms'' controlling regional climate. Diagnosing where and when these regional engine rooms are active is the second objective of this paper.

Section 2, which follows, outlines the data and methods that underpin the rest of the paper. This section also provides motivation for studying widespread convection as specifically distinct from African rainfall. The presentation of the results is organized to address three central aspects of widespread convective activity across Africa:

- the annual cycle of convection across the continent (section 3),
- the impact of ENSO on pan-African convective activity and highlight hotspots of deep convection (section 4), and
- contemporary changes in mean convective activity across Africa (section 5).

Section 6 provides a summary of the salient results and the paper closes with conclusions that are drawn from these findings.

2. Diagnosis of widespread convective activity

The redistribution of energy by deep convection is a defining characteristic of the local and regional atmospheric circulation and water cycle across much of Africa, as in the global tropics, and is achieved both vertically and horizontally by complex interplays between latent heating, radiative cooling, and momentum transport through the full depth of the troposphere [for a review, see Roca et al. (2010)].

In many studies, rainfall serves as a proxy for diabatic heating of the column. However, difficulties in estimating rainfall without an extensive rainfall station network, even with satellite observations (e.g., Maidment et al. 2015; Awange et al. 2016), continue to hamper research efforts focused on African weather and climate. These difficulties are greatest in the most convectively active part of the continent, the Congo, where observations are sparse (Washington et al. 2013), and even recent datasets (Nicholson et al. 2018) have resolutions below those necessary to consider widespread convection directly. Irrespective of these difficulties, rainfall is good a proxy for the diabatic heating rates of deep convection, but it does not necessarily diagnose radiative cooling controlled by deep cloud (e.g., Fiolleau and Roca 2013).

Therefore, there is a strong rationale for an alternative proxy to diagnose deep convection in a way that summarizes the full potential of such convection to modify regional to global circulation. Such a proxy should highlight widespread convection rather than isolated convective cells, as it is organized mesoscale convection that is particularly effective at impinging on large-scale circulation in both the tropics (Houze 1982; Hartmann et al. 1984) and the extratropics (Rodwell et al. 2013).

A key character of such organized convection is the cold cloud shields which develop characterized by tropopause-level cirrus and the even colder (deeper) clouds associated with the core convective updrafts. These cold cloud characteristics have been exploited in mesoscale convective system tracking algorithms typically applied to 15-min to 3-hourly data (e.g., Hodges and Thorncroft 1997; Carvalho and Jones 2001; Laing et al. 2011). However, mesoscale convection systems are a specific subclass of widespread convection (Houze 2004). They form a crucial part of convective activity, and indeed rainfall, over Africa, but are not the whole (Jackson et al. 2009; Laing et al. 2011; Roca et al. 2014). Our study seeks to answer questions about widespread deep convection more generally. Answering these questions requires a summary diagnostic that provides a daily integral of deep convective activity across the continent.

a. Data

This integral of deep convection is provided by using the thermal infrared radiation observations made onboard the Meteosat geostationary satellites to compute daily cold cloud duration (CCD). CCD is expressed as number of minutes a pixel exhibits temperatures below a chosen brightness temperature threshold. Maidment et al. (2014) provides full details of a climate data record of CCD computed from thermal infrared imagery detected by Meteosat first- and second-generation satellites. CCD values for cloud brightness temperatures below −30°, −40°, −50°, and −60°C were computed. This dataset underlies the TAMSAT (Tropical Applications of Meteorology using Satellite and Ground-Based Observations) product, which provides a long-term stable and routinely updated estimate of African rainfall long-term stable and routinely updated estimate of African rainfall (Maidment et al. 2014, 2017). The climate record quality of this CCD data, computed on a 0.0375° latitude–longitude grid (~4 km) and used here for the 1983–2015 period, provides an appropriate dataset to answer the questions posed in this paper. CCD provides an effective integral of daily convective activity across Africa and is a more direct diagnostic of convection than rainfall, minimizing the additional uncertainties introduced by satellite-derived rainfall estimation.

A large-scale summary of the thermodynamic environments supporting convection across Africa is obtained by computing monthly mean moist static energy (MSE) from moisture and temperature variables estimated in the NCEP–DOE Reanalysis II (NCEP2; Kanamitsu et al. 2002). These data are available on a 2.5° × 2.5° latitude–longitude grid. Low-level MSE was diagnosed using variables on the 850-hPa level. Due to estimation from reanalysis, which is poorly constrained in data-sparse parts of Africa, especially the Congo (Hua et al. 2019), this MSE should only be treated as indicative of the climatology for the continent.

The ENSO events considered in this study are obtained from years in which the Niño-3.4 SST anomaly peak exceeds $\pm 0.7\sigma$ of a standard deviation from climatology during 1983–2015. The NOAA Optimally Interpolated SST (OISST) was used to create this index (Reynolds et al. 2002). The El Niño events considered begin in 1986, 1987, 1991, 1994, 1997, 2002, 2006, and 2009 with La Niña events in 1983, 1984, 1988, 1995, 1998, 1999, 2000, 2007, 2010, and 2011.

b. Methodology

The goals of this study focus on widespread convection, especially convection that is of sufficient scale to

have an impact on regional circulation. The CCD brightness temperature threshold of −50°C is chosen for use here as it is a well-established value appropriate for the identification of mesoscale convective systems (Jackson et al. 2009; Laing et al. 2011; Blamey and Reason 2012). Figure 1 provides examples of this assertion: brightness temperatures lower than −50°C (dark blue) capture convectively active cloud shields, whereas the −40°C threshold (light blue) includes cirrus outflow. Such low brightness temperatures rarely last long in one location so a duration threshold of more than 30 min is applied to the CCD field at −50°C (CCD_{50}) to identify deep convection. Changing these thresholds modifies the magnitude of values output by the analysis in this study, but has negligible impact on climatology and interannual variability results in terms of when and where the most convection is observed. However, reported trends in convective activity are greater for the colder brightness temperature thresholds, as reported in the literature (Taylor et al. 2017; Raghavendra et al. 2018). This will be discussed in section 5 and figures reproduced with the −60°C CCD data are included in the online supplemental material.

While CCD_{50} is an appropriate threshold for identifying the cloud shields of organized convective systems, this field does not summarize how widespread convection is in a region. To obtain this summary, we compute a convective coverage ratio defined as

$$\text{ccratio} = \frac{a}{\pi r^2}, \tag{1}$$

where a is the area of $CCD_{50} > 30$ min within a circle defined by radius $r = 1°$ of latitude. This ccratio calculation is applied to the 4-km gridded CCD_{50} and is only computed at every grid point on a 0.5° latitude–longitude grid. The output is a coarse-grained diagnostic of daily convection that preferentially highlights widespread outbreaks of convective activity. This diagnostic is very similar to the output of regridding the CCD data to 0.5° using a spatial smoother such as a bivariate spline. However, that approach loses the localization over high-intensity orographic convection hotspots. The ccratio retains this localization. Monthly means of this metric are used to show the spatial and seasonal variation of widespread convective activity across the continent. The monthly mean of the ccratio quantifies the joint probability of the frequency and spatial extent of deep convection. For example, the ccratio would be 0.5 if 100% of the circle were covered by deep convection during half of the days in a month. The value of 0.5 would also be diagnosed if 70% of 1° circle surrounding a grid point were covered by deep convective cloud during two-thirds of days in a month. Thus, the monthly mean ccratio represents a simple way to diagnose the mean activity of widespread convective outbreaks.

A complementary object-based analysis was performed on the CCD_{50} data in order to explicitly separate long-term changes of areal extent from long-term changes in number of convectively active days. A standard connected component labeling algorithm (van der Walt et al. 2014) was applied to each daily $CCD_{50} >$ 30 min thresholded image. The ''blobs'' output from the algorithm were used to build a database of convective objects including area and location. These properties were then used to compute the monthly mean areal extent of convective objects and the total monthly count of these objects in convective activity hotspots. Long-term changes were computed from these means (presented in section 5).

3. Annual progression of deep convection

September, the start of boreal autumn, is the month in which convection starts to progress southward across the continent as the West African peak of convection wanes. As such, we commence our analysis of the spatial migration of convection in this month.

a. *Where and when is there widespread convective activity?*

In September, large convective systems develop across West Africa, while widespread deep convection starts to extend southward into the Congo River basin (Fig. 2). This extension closely matches the rapid southward migration of the latitude of maximum solar heating during September as shown by the latitudes of the solar zenith on the first and last days of the month are indicated in Fig. 2. Theory and observations show that the latitude of maximum tropical convection is to the first order controlled by the maximum surface moist static energy (MSE) (Neelin and Held 1987; Nie et al. 2010). The seasonal migration of the solar zenith is an important control on this MSE maximum and is therefore shown for reference on Figs. 2 and 3, along with contours for high MSE. To reiterate what was noted in section 2a, these MSE values should be interpreted as a useful but poorly constrained estimate of the natural system since observations are so sparse in the region.

In October, southward migration of the rain belt brings widespread convective activity into southern Congo and Angola. A hotspot of activity develops along the Rwenzori-Virunga Mountains, the eastern boundary of the Congo basin (Fig. 2; October panel), with ccratio values > 0.5. Notably, these convective episodes are confined to the west of the subcontinent. Widespread

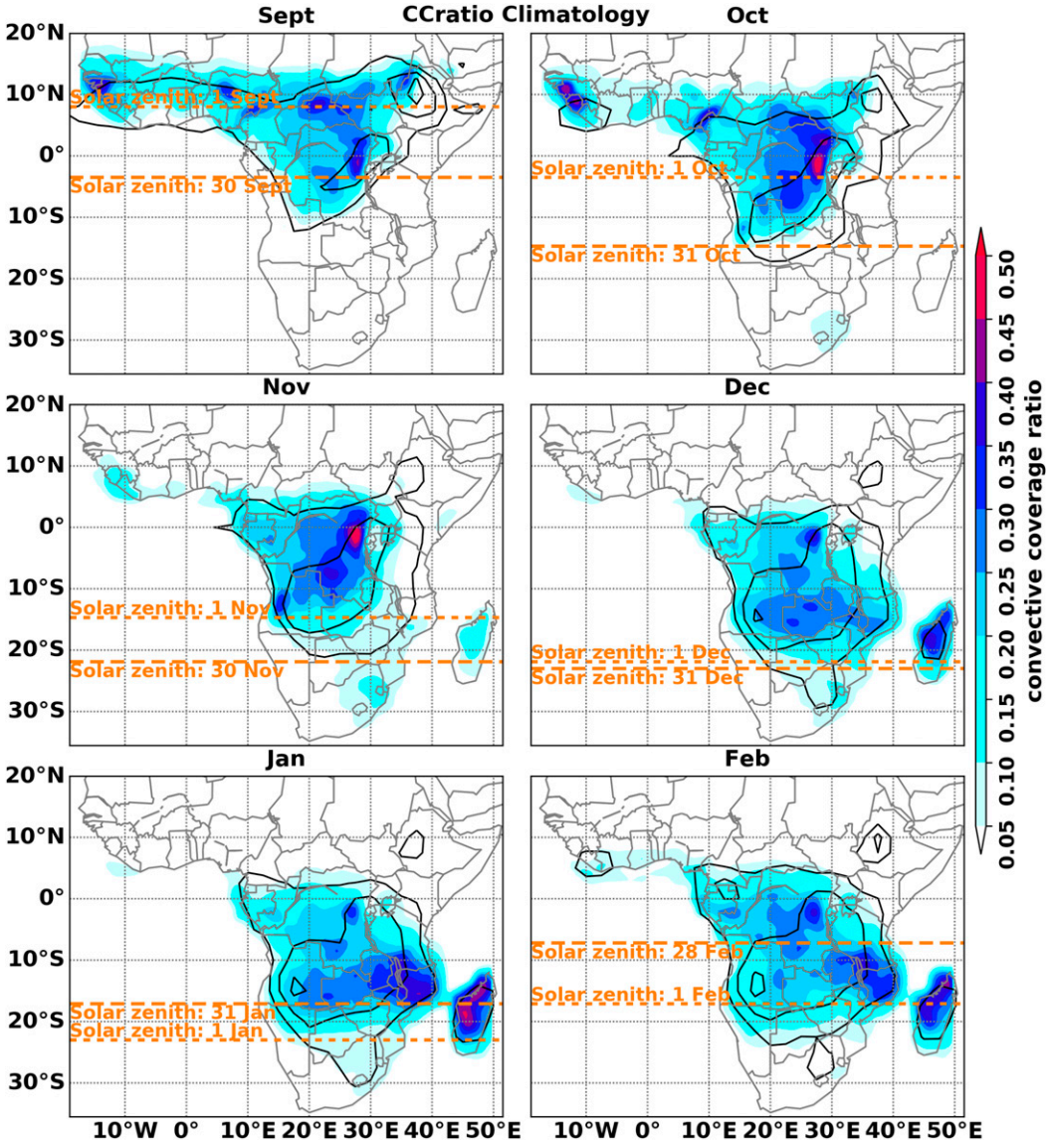

FIG. 2. September–February climatology (1983–2015) of monthly mean convective coverage (shading). Climatology of highest low-level (850 hPa) moist static energy contoured at 340, 345, and 350 kJ (black lines).

convection fails to form in East Africa where MSE remains lower than in central Africa. The exception in convective activity is the small region on the southeastern coast near 30°S where convective outbreaks are occasionally observed (Fig. 2) in October. Such outbreaks are often supported by short episodes of synoptic-scale uplift in response to tropical–extratropical interactions (Hart et al. 2013).

Convective hotspots over the Angolan Highlands and East Congo are prominent in November (Fig. 2), despite the latitude of maximum solar heating moving well south of these locations by the end of the month. The more southerly position of the solar zenith provides the necessary forcing to support widespread convective episodes along the eastern half of subtropical southern Africa and Madagascar. The subtropical convective activity in southeastern southern Africa is further invigorated in November and December as low-level MSE increases (Fig. 2). This is the peak season for the organization of convection into mesoscale convective complexes over the lowland plains of South Africa and Mozambique (Blamey and Reason 2012).

During December, the most frequent convective outbreaks establish over countries along the southern tropical edge, broadly located between 10° and 20°S (Fig. 2). This includes enhanced outbreak activity over

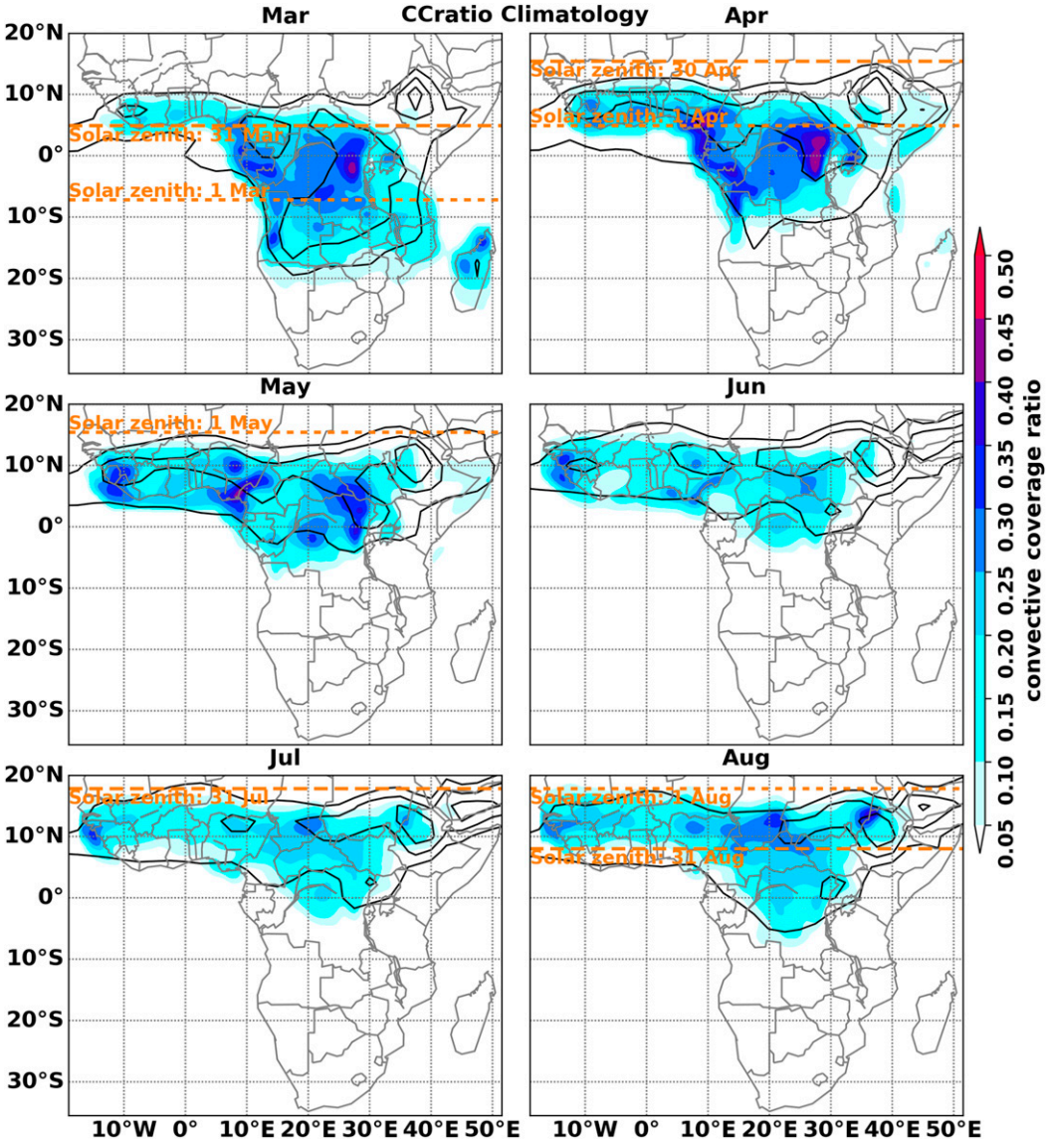

FIG. 3. March–August climatology (1983–2015) of monthly mean convective coverage (shading). Climatology of highest low-level (850 hPa) moist static energy contoured at 340, 345, and 350 kJ (black lines).

Madagascar with ccratio values exceeding 0.35. Diminished convective activity over the Angolan Highlands and East Congo hotspots is associated with the enhanced convective outbreaks along the tropical edge farther south.

Figure 2 shows that the most vigorous and persistent convective activity during January and February is found across eastern southern Africa. Zambia, Malawi, Tanzania, Mozambique, and Madagascar become a regional hotspot for large-scale convective outbreaks. This region is known for intense tropical depressions that occasionally develop into tropical cyclones (Mavume et al. 2009; Rapolaki and Reason 2018). This activity is associated with the large values of low-level MSE in the region.

During March, the northward movement of the solar zenith is associated with a decrease in MSE, widespread convection in the eastern subcontinent, and invigoration of large outbreaks in Congo basin and along the west coast of equatorial Africa (Fig. 3). Invigoration of widespread convection along the tropical west coast is amplified further in April, as is activity in the East Congo (Fig. 3). The Angolan Highlands and Madagascar maintain local convective hotspots during March, but by April these have subsided (Fig. 3). Convection becomes widespread along the west equatorial African

coast in May (Fig. 3) with concentrations over the highlands of Cameroon and Guinea including parts of Sierra Leone and Liberia.

During June, convective activity is confined to the Sahel despite the solar zenith lying well north in the Sahara (Fig. 3, out of the frame). This moisture limitation north of ~15°N is reflected in the low-level MSE with the 340-kJ contour effectively bounding the West African monsoonal convection. Similar to June, July (Fig. 3) has lower values of convective coverage (ccratio = 0.15–0.25) when compared to values observed in central and southern Africa (ccratio = 0.25–0.40) in peak warm-season months (Fig. 2). If the frequency of convective outbreaks in both regions were similar at 10 days month^{-1}, these values would indicate a typical spatial convective coverage of 100% over the eastern southern Africa hotspot versus 70% over West Africa, during the core months in each region. This is in part due to the low-level MSE, which rarely exceeds 345 kJ, in contrast to southern Africa in January and February where MSE is widely above that value (Fig. 2).

The return of the latitude of maximum solar heating to the Sahelian belt, during August, enhances widespread convective activity (Fig. 3) by ~20%. This invigoration is particular prevalent in hotspots in southern Chad and on the northwest edge of the Ethiopian Highlands (Fig. 3d). Early indication of the start of the Congo basin convection season is also observed in August.

Figures 2 and 3 demonstrate that the seasonal march of widespread convective outbreaks across Africa has marked asymmetries and distinct convective hotspots. The southward progression of convective activity during September–November is confined to the western parts of the continent associated with geographic asymmetries in rainfall onset reported in Dunning et al. (2016). During the core austral summer months (December–February) the convective rain belt extends across the southern tropical edge countries of southern Africa with the most extensive convective outbreaks observed in the east, adjacent to the Mozambique Channel. This dominance of widespread convection in eastern southern Africa persists into March as the rain belt returns northward during the onset of boreal summer. The patterns of onset and peak convective activity in boreal summer (June–August) have a markedly more even distribution across the zonal extent West Africa than those over southern Africa.

b. When is pan-African convection most vigorous?

The obvious differences in the extent of deep convective activity in Figs. 2 and 3 are further investigated in Fig. 4. Here, the histogram of ccratio values from all grid points across the continent is computed for each month. The dashed gray curve shows the annual average for reference (Fig. 4).

September shows a peak in moderate ccratio values (ccratio ≈ 0.22), but in October convective activity the distribution is weighted to more widespread activity. This is demonstrated by the fewer grid points with ccratio values below 0.25, when compared to the annual average, but more grid points with values above 0.25 compared to the annual averaged (Fig. 4; October panel). April has an even more pronounced version of this pattern with substantially more widespread deep convection for those grid points that are convectively active (Fig. 4; April panel). October and April (Fig. 2) are also months in which convection is particularly confined to the Congo basin.

The combination of widespread convection concentrated in the tropical center of Africa suggests that these transition-season months may be periods during which African tropical convection has the greatest potential impact on global circulation climatology. This transition-season convection is also closely linked to the bimodal peak in equatorial African rainfall (Washington et al. 2013; Awange et al. 2016). This is in contrast to the June–July period (Fig. 3), when organized convection is spread widely across West Africa with generally lower values of convection coverage (Fig. 4) compared to the annual mean.

Figure 4 shows, however, that January–March has more widespread convection across all magnitudes of the ccratio. As noted previously, Tanzania, Malawi, and Mozambique host much of this convection during January and February, with the eastern and western Congo playing host in March, and into April (Fig. 3). This late austral summer activity is dominated by central African convection and lingering activity in the southeast. This is the period of highest convective activity across the continent as a whole, as discussed next.

What is the annual cycle of deep convection for the continent as a whole? The pan-African mean convective activity is shown in Fig. 5a. March and April see more widespread convection, averaged across the continent, than at any other time of the year. This pan-African activity peaks as the central African hotspots become most active in austral autumn. In contrast, the June and July core months of the West African monsoon have the lowest values of pan-African convection (Fig. 5a). This is a result of the lower values of convective coverage across a narrower zonal band through West Africa, with little activity in central Africa (Fig. 3).

To summarize, pan-African activity in widespread convective outbreaks is at a peak in late austral summer during March. The combination of intensity and

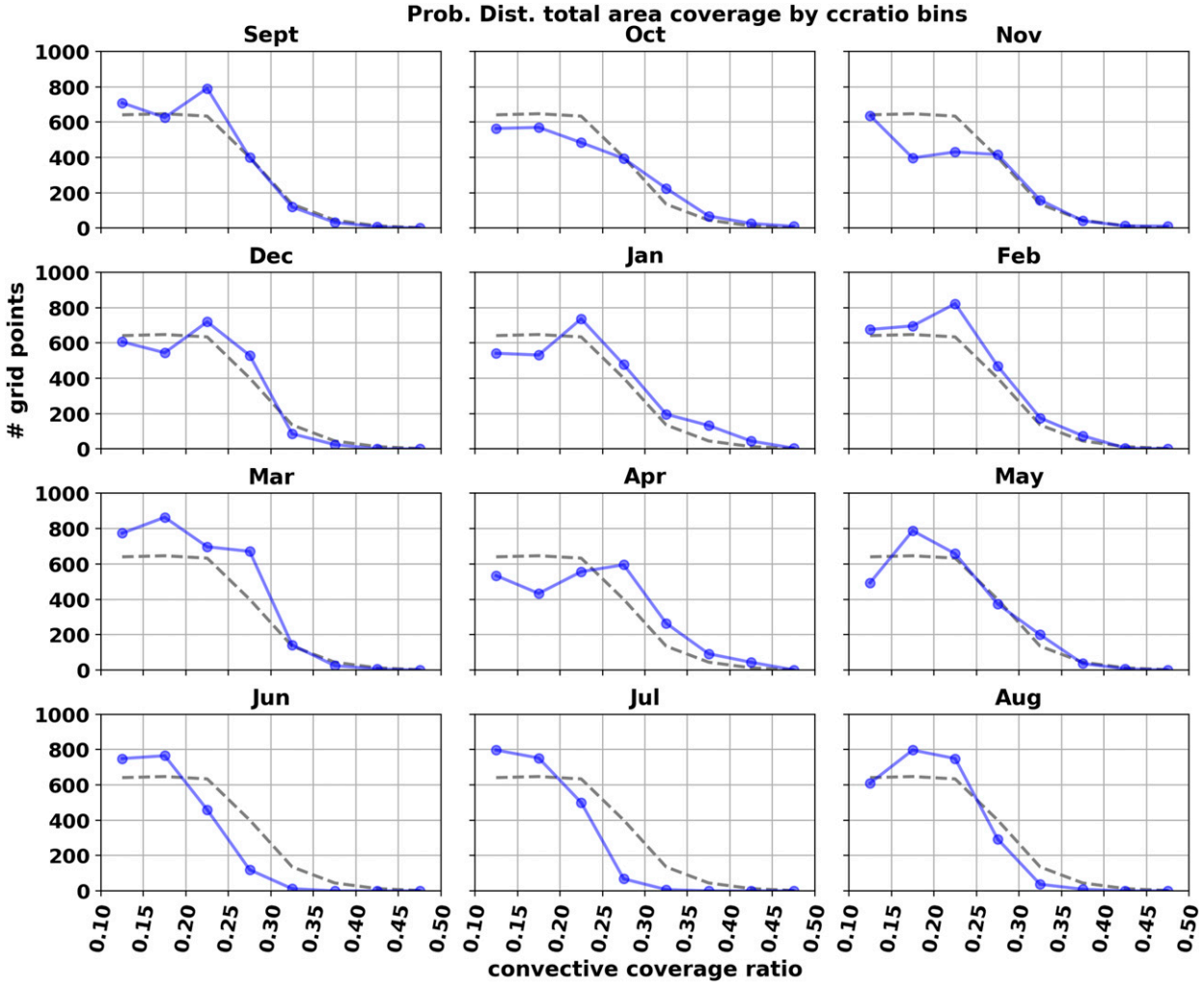

FIG. 4. Probability distribution of widespread convective coverage values across Africa for each month (blue lines). The annual mean distribution is shown for reference (gray dashed line).

geographic coherence of this activity in these transition months of March–April, as well as October to some degree, suggests that these are the periods when African convection has the greatest potential to influence the global general circulation.

4. The effect of ENSO on African convection

On interannual time scales, the strongest modification to the annual cycle of the global climate happens during El Niño–Southern Oscillation (ENSO) events (e.g., Bjerknes 1969; Rasmusson and Carpenter 1982). For many parts of Africa, ENSO is the first-order control on interannual variability of the warm-season rainfall (Ogallo 1988; Lindesay 1988; Ward 1992). SST variability in adjacent ocean basins has strong impact too; however, much of this variability is intimately tied to ENSO variability (Nicholson and Kim 1997). This study therefore considers only this first-order impact on the annual cycle of African deep convection.

Figure 5b shows that ENSO has a distinct impact on pan-African convective activity. The interquartile ranges shown are for annual cycles computed from August through July to consider the development of the ENSO event during austral spring, the maximum tropical Pacific SST anomalies in austral summer, and the decay during austral autumn. For pan-African convection, El Niño events demonstrate a general suppression of the annual cycle relative to La Niña events (Fig. 5b). The climatological peak in March is reduced and the lower activity during June and July is lowered further. The equally plausible alternative view is that these features of the annual cycle are enhanced during La Niña events. As will be shown next when viewed through

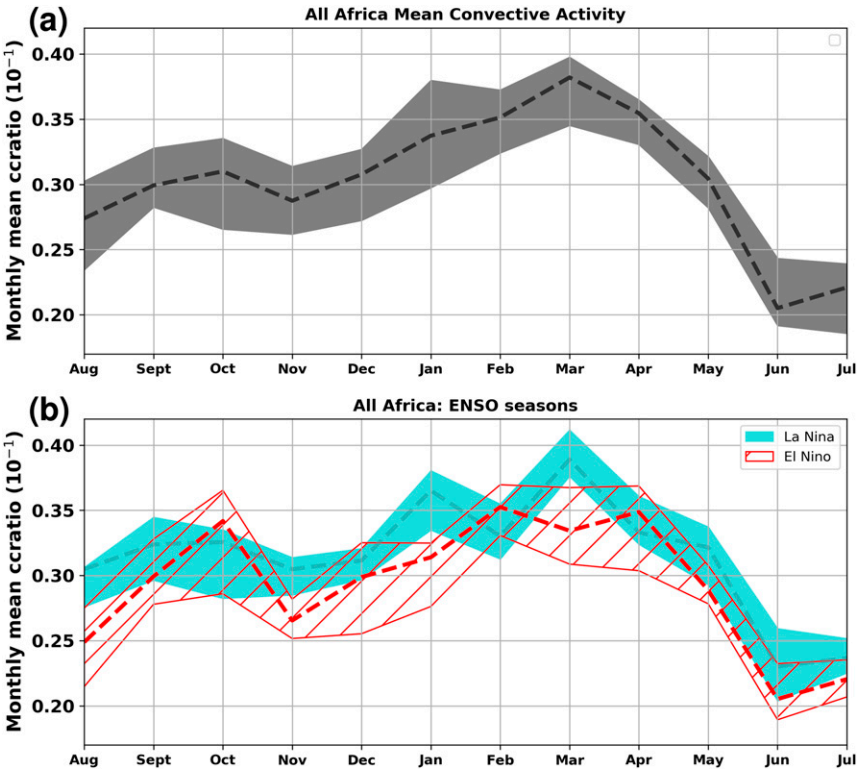

FIG. 5. (a) The annual cycle in pan-African monthly mean convective activity depicted by the median (dashed line) with the interquartile range shaded in gray. (b) Seasons in which La Niña events (light blue shading) and El Niño events (red hatching) developed, as shown by the interquartile range in monthly mean ccratio. The median is shown in dashed curves. Seasons are considered from August to July during which ENSO-related SST anomalies reach a maximum in austral summer.

anomaly maps, the response shown in Fig. 5b is a combination of both responses.

a. Where is the ENSO response the strongest?

1) EL NIÑO COMPOSITE

The composite response in widespread convection over Africa to El Niño events is spatially and temporally complex due to inter-ENSO event diversity and the stochasticity inherent in outbreaks of organized mesoscale convection (Fig. 6). Nevertheless, robust signals emerge in each month that have similarity to the broad understanding of the regional response to El Niño. Note that the false detection rate as used here [after Ventura et al. (2004)] results in p values ~0.01, so the shaded values are composite responses that are robust despite high levels of noise between different El Niño season responses.

During September of developing El Niño events, there is a weak and spatially discontinuous reduction in organized convective activity throughout the rain belt, consistent with the pan-African signal in Fig. 5b. This response switches in October to a weak enhancement of possible widespread outbreaks (Fig. 6). By November, a more coherent pattern emerges with enhanced convective activity over East Africa, at the expense of activity in the Congo and subtropical southern Africa. During December, the enhancement over east Africa intensifies over Tanzania with strong reductions in widespread convection along the southern edge of the tropical rain belt (Fig. 6). The widely reported (e.g., Nicholson and Kim 1997; Dunning et al. 2016) East African rainfall dipole response—drying in the south with wetting in the northeast—is manifest here in December. Malawi and northern Mozambique are the fulcrum of this response in convection. Southern Zambia, Zimbabwe, Malawi, Mozambique, and southern Madagascar all have reduced convective outbreak activity. Northeastern South Africa has a significant increase in the likelihood of widespread convection. In January, widespread convection is reduced in the region of the Angola low (Reason et al. 2006; Howard and Washington 2018) over northern Botswana and Namibia, with vigorous outbreaks over Madagascar (Fig. 6).

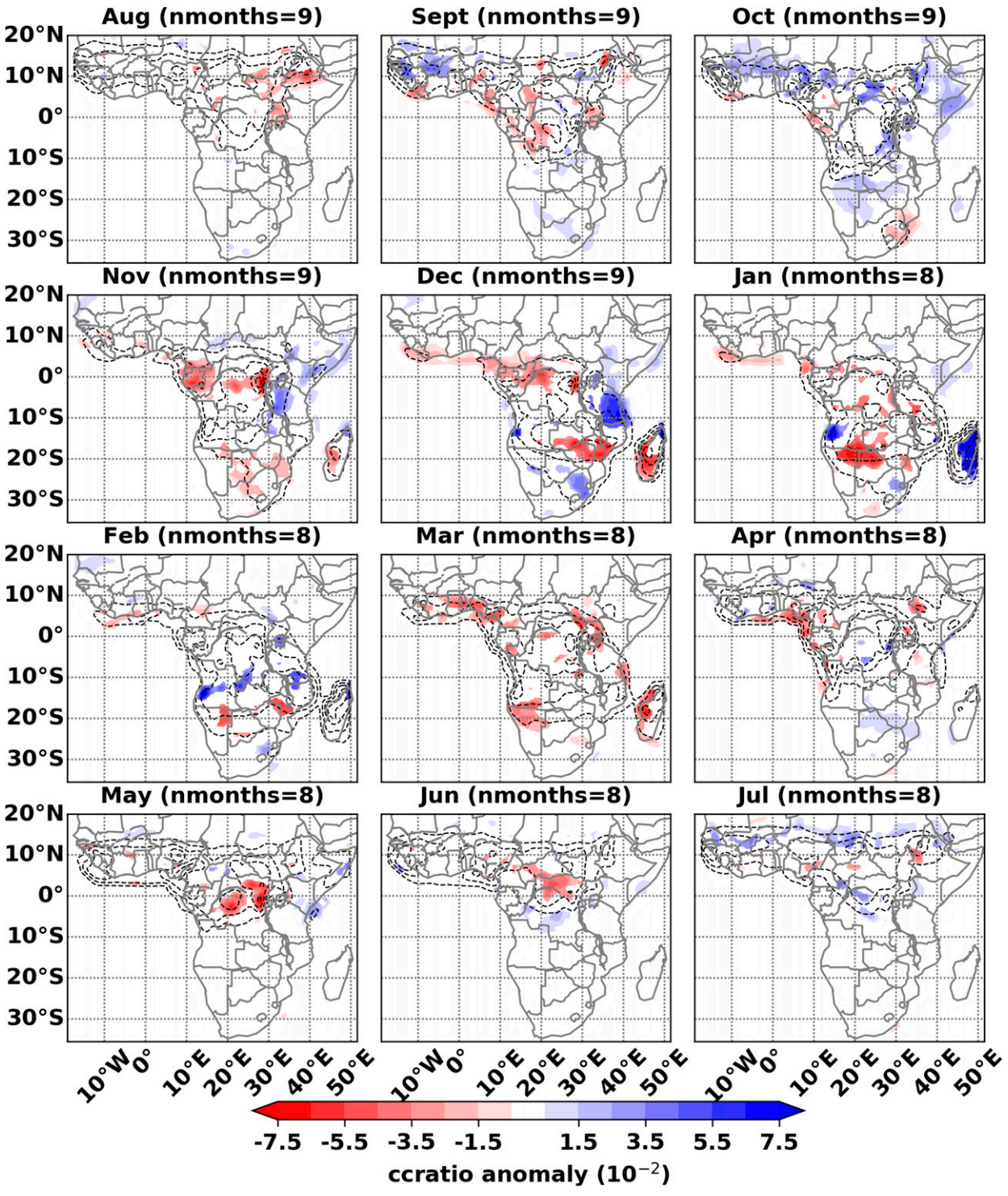

FIG. 6. Composite anomalies in monthly mean convective coverage during El Niño events sequenced from developing phase in September. Anomalies are only shaded where statistically significant as determined by a Student's t test with the false discovery rate controlled by the p^*_{FDR} value computed with $\alpha_{\mathrm{FDR}} = 0.1$. For reference, the mean climate of ccratio, as in Fig. 1, is contoured from 0.05 at 0.1 increments (black dashed).

During February, the spatial coherence of the El Niño response is lost but significant reductions in convective outbreaks are seen over northeastern Namibia and Zimbabwe, with increases over the Angolan Highlands, southern Congo, and Tanzania (Fig. 6). Central Malawi again acts as a fulcrum between enhanced convection to the north and reduced to the south. By March convective outbreaks are reduced in regions peripheral to the convective core over the Congo, particularly in northern Namibia and Madagascar and along the central West African coast (Fig. 6).

As the rain belt moves north during the decaying months of the El Niño events, small but significant decreases in convective activity are noted over western equatorial Africa in April (Fig. 6). In May and June, significant decreases are seen in northeastern Congo. By July, there are weak indications of increased activity across the Sahel, but again the spatial coherence is weak (Fig. 6).

2) La Niña composite

The final months of the West and North African wet seasons experience enhanced widespread convection during the development of La Niña events, as shown in the August to October panels of Fig. 7. However, coherent anomalies in convective activity do not develop in southern Africa until January. The climatological hotspot for convection in eastern southern Africa is strongly amplified with more frequent and widespread convection over Mozambique, Malawi, and Tanzania, with a reduction to the west over the Angolan Highlands (Fig. 7).

During February of La Niña events, convection at the southern tropical edge is enhanced associated with a reduction of widespread convection across Angola, the Congo, and southern Tanzania (Fig. 7). The Malawi fulcrum in the wetting and drying signal seen during El Niño is also manifested in La Niña during February. However, during March increased widespread convection is likely throughout northern Mozambique, Malawi, and Tanzania. Small reductions in March convective outbreaks are also noted near the Angolan Highlands and eastern Congo (Fig. 7).

The northward migration of the rain belt during April of La Niña events is accompanied by strongly enhanced activity of organized convection over west equatorial Africa (Fig. 7). This enhancement persists along the West African coast during May and extends across the convective regions of North and West Africa during June and July (Fig. 7, June and July panels). It is this enhancement that is seen in the pan-African convective activity for June and July, relative to El Niño seasons (Fig. 5b).

Overall the response of widespread convection to ENSO events is similar to the rainfall response (e.g., Nicholson and Kim 1997), but appears more complex. This, however, is largely due to month-by-month analysis here. The wetting in East Africa drying in southern Africa summary ENSO signal emerges most clearly in seasonal mean anomalies [e.g., October–March as in Dunning et al. (2016)]. But this summary signal hides the noise inherent in the ENSO response from month to month, as demonstrated in Figs. 6 and 7.

The southern African summer response to ENSO has a clear fulcrum between enhanced and reduced convection located over central Malawi and northern Mozambique. The presence of the convective hotspot located in the southeastern Africa during December–February (Fig. 2) predisposes this region to exactly such a response. A hotspot bounded north and south by low convective activity will have north–south wanderings manifested as a north–south dipole in anomalies. The anomalies here show that this hotspot tends to locate farther north during El Niño particularly in December and January (Fig. 6), whereas during La Niña the hotspot has amplified activity throughout January–March with a shift to the south during February (Fig. 7). Interevent variations in the magnitude of the shift during ENSO results in a fulcrum region shown by blank shading separating the dipole anomalies. In these regions, the response to a given ENSO event is highly uncertain both at the seasonal and subseasonal time scales.

b. Identification of deep convection hotspots

Analysis of the regional distribution of convective activity (section 3) and ENSO-related variability (section 4a) highlighted convective hotspots across the continent. We now investigate the seasonality, variability, and change in these hotspots. Figure 8 shows the monthly mean widespread convective activity for the month in which climatological convective activity is greatest. This peak is computed individually at each grid point (shading) and the associated year-to-year standard deviation in convective activity for that corresponding peak month is shown in contours (Fig. 8). This figure shows the hotspot regions chosen due to either local maxima in widespread deep convective activity (shaded) or high interannual variability (contours) in peak convective activity.

Unsurprisingly, the convective activity hotspots and interannual variability hotspots are often coincident. These hotspots represent areas likely to receive substantial convective rainfall, which for the high-elevation hotspots is crucial to the head waters of regional rivers. Furthermore, given the spatial and temporal scale of

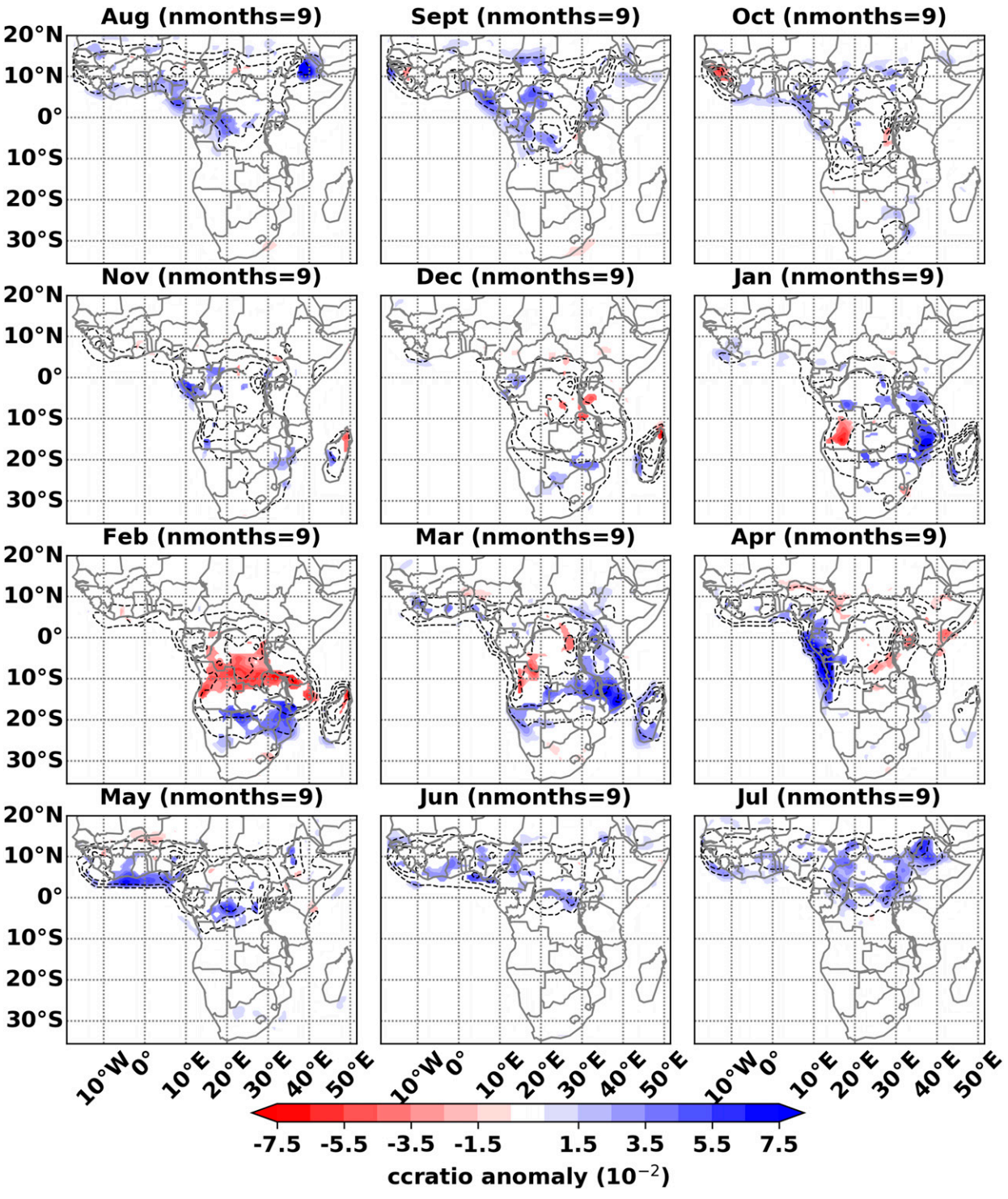

FIG. 7. As in Fig. 6, but for La Niña events.

convection diagnosed with this metric, it is likely that convective activity in these hotspots influences circulation on regional scales. Hotspots considered further are indicated by the boxes in Fig. 8.

We briefly note that there is potential to define a hotspot over a region in eastern Chad (15°N, 22°E), especially with regard to interannual variability in convective activity (Fig. 8). This roughly corresponds to the

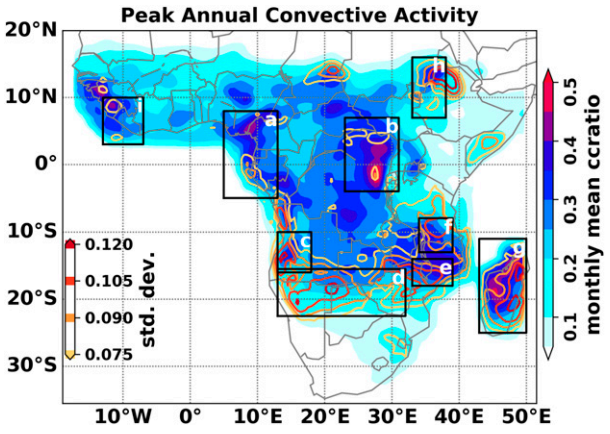

FIG. 8. Peak monthly mean convective activity for each grid point (shaded) and the associated standard deviation in convective activity for that corresponding peak month (contours). Boxes indicate hotspots considered in the annual cycle plots in Figs. 9 and 11–13.

Darfur MCS hotspot shown by Jackson et al. (2009). This hotspot and the Ethiopian Highlands display similar annual cycles in convective activity and—as will be noted in section 5—similar contemporary increases in peak season activity.

c. What is the effect of ENSO on the annual cycle of convection in the hotspots?

The two equatorial hotspots, west equatorial Africa and east Congo, have a bimodal seasonal cycle in convective activity with relatively low interquartile range through the annual cycle (Fig. 9). These correspond to the MCS activity hotspots studied in Jackson et al. (2009). West equatorial Africa has significantly less widespread convection during El Niño than during La Niña. This is expressed during the developing stages (September–November) and decaying stages (April–May) of ENSO events, coincident with the two annual peaks. Convective activity in the East Congo is similarly reduced during May and June of decaying El Niño events.

Over the Angolan Highlands, the November and March peaks in widespread convective activity are unaltered during ENSO events. However, La Niña seasons have distinctly lower convective activity during midsummer, relative to El Niño years. As noted in section 4a, this demonstrates that the rain belt makes a great excursion into the subtropics during La Niña seasons and remains deeper in the tropics during El Niño seasons. This behavior is well captured in the convective activity along the southern African tropical edge: La Niña seasons have substantially enhanced widespread convection relative to El Niño seasons (Fig. 9d).

Section 4a discussed how the mid- to late summer ENSO impact was pronounced in the eastern southern Africa, as shown in the composite maps in Figs. 6 and 7. As discussed in section 2, there is only one hotspot here, but the nature of variability creates a response region to the north and the south. This impact is shown in Figs. 9e and 9f with a reduction in convective activity over southern Malawi and Mozambique during January of El Niño seasons and enhanced activity during February in southern Tanzania, relative to La Niña. However, the ENSO response in these two regions is highly unreliable as shown by the widest interquartile ranges in convective activity of all the hotspots across the continent (Fig. 9). These interquartile ranges show that from December through February, the measure of widespread convective activity can vary by up to 50% of the full annual range. Such variability is likely a combination of the strong ENSO influence here (Figs. 6 and 7) and likely geographic variation in the position of the fulcrum of the wet–dry dipole during individual ENSO events.

In contrast to the wide range of response over eastern southern Africa, Madagascar shows a clearer modification of the annual cycle in convection during ENSO events. The interquartile ranges show enhanced convective outbreaks during January of El Niño seasons; however, this cannot be deemed statistically distinct from the range observed during La Niña events.

The impact of ENSO on East Africa north of the equator is seen over the Ethiopian Highlands, where outbreaks of widespread convection are enhanced in La Niña seasons relative to El Niño years, during the peak activity months of May, July, and August (Fig. 9h). The Guinea hotspot, as shown in Fig. 9i, is the only hotspot with no discernible impact from ENSO events in any months.

5. Contemporary changes in African convection

There are a number of studies that demonstrate substantial changes in rainfall, including local increases, during the satellite observation record from 1980 to the present (e.g., Maidment et al. 2015). Increases in intense MCSs and associated rainfall extremes have been particularly pronounced in some locations (Taylor et al. 2017, 2018). Are such increases in convective extremes are reflected in the mean climatology of widespread convective outbreaks? We answer this here by considering the continental-scale mean and focusing on the convection hotspots highlighted in Fig. 8.

Indeed pan-African widespread convection has increased by ~10% over the last 30 years, shown by the low-pass-filtered (blue dashed) annual activity in Fig. 10a. Intriguingly, this increase is well matched by the growing asymmetry between the Northern and

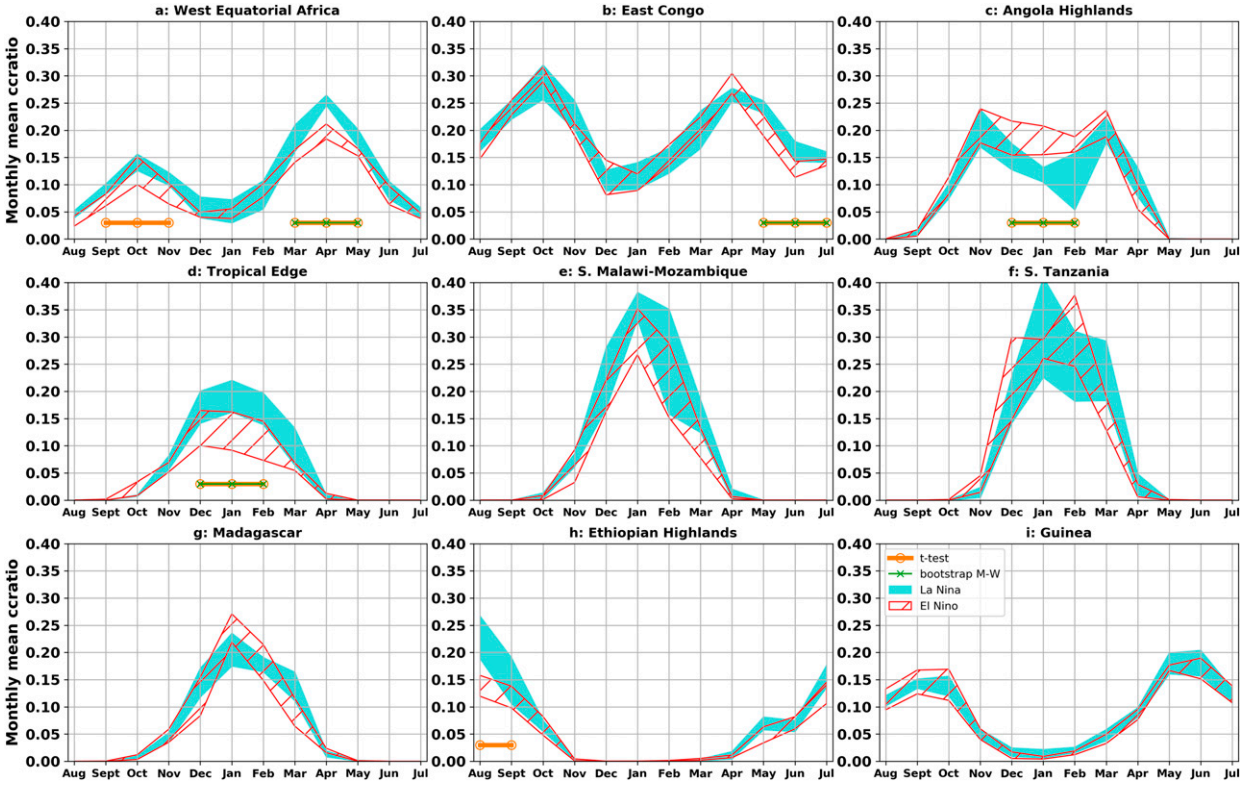

FIG. 9. ENSO impact on the annual cycle of area-averaged convective coverage ratio for the convection hotspots of the African rain belt (see Fig. 8). The interquartile range of monthly mean convective coverage is shown by the width of the curves for seasons that occurred during La Niña events (light blue shading) and El Niño events (red hatching). Seasons are considered from August to July during which ENSO-related SST anomalies reach a maximum in austral summer. Periods in which El Niño and La Niña observations have less than a 5% chance of being drawn from the same distribution, as determined by a bootstrapped Mann–Whitney *U* rank test, are indicated by a green line. Significance is additionally considered with a *t* test (orange curve).

Southern Hemisphere averaged surface temperatures (gray curve in Fig. 10a). Taylor et al. (2017) noted the asymmetric increase in North African temperatures with Zhou (2016) and Zhou et al. (2016) demonstrating the higher magnitudes of surface warming across the Northern Hemisphere. The result in Fig. 10a demonstrates an association with the interhemispheric asymmetry related to the mean temperature of whole Northern Hemisphere. The increase in annual mean activity is distributed across all months as shown in Fig. 10b by the differences in the interquartile ranges of monthly convective activity between the first (orange) and second (blue hatched) half of the record. The largest increase is from June to August and, as will be shown next, this is associated with enhanced convection in the East Congo, Ethiopian Highlands, and Guinea.

Contemporary changes in the annual cycles of African convective hotspots

Contemporary trends in African rainfall have been addressed by a number of authors, with most recent results demonstrating increases in groundwater reserves—with a few decreases—in local regions across Africa (Rodell et al. 2018). This section specifically considers contemporary changes in the primary convective hotspots on the continent. As noted before, the changes in large-scale convective outbreaks over the hotspots would have implications for the regional water balances and potentially profoundly impact regional circulation.

Figure 11 confronts the question whether hotspot annual cycles of convective activity sampled during 2000–15 are distinct from activity observed between 1983 and 2000. Many of the hotspots have seen increased activity in widespread convection. Along western equatorial Africa, the increase is visible in the interquartile ranges from November through February (Fig. 11a). In the East Congo, there have been notable increases in the mean convective activity in February—Taylor et al. (2018) showed robust February increases of the most intense MCSs—but the most significant increase has been during June–August. This increase makes an important contribution to the pan-African JJA increase shown in Fig. 12b. Paradoxically, rainfall has been reported decreasing in

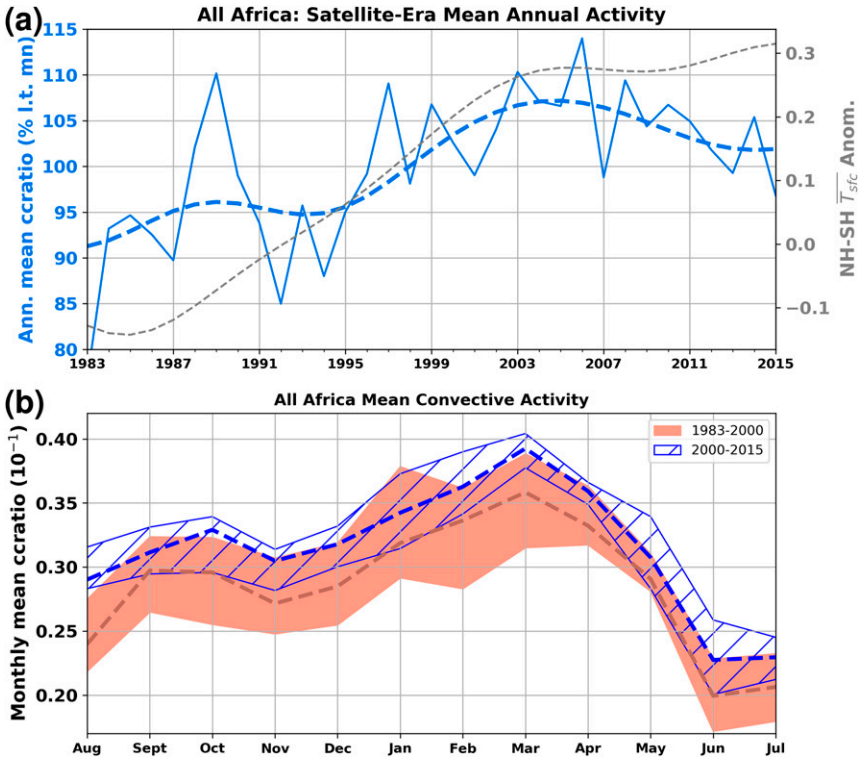

FIG. 10. (a) The annual mean of pan-African convective activity for the geostationary satellite record since 1983 (solid blue). A Butterworth filter is applied to only retain the low-frequency variation (>6 yr) across the period (blue dashed). The low-pass-filtered interhemispheric surface temperature difference for the same period is shown with a gray dashed line. (b) The distribution of this change across the annual cycle. The interquartile range of monthly mean convective coverage is captured by the width of the curves for the 1983–2000 period (coral shading) and the 2000–2015 period (blue hatching). The median is shown with dashed curves.

East Congo (Zhou et al. 2014). Raghavendra et al. (2018) has proposed that this paradox should be understood as taller and narrower convective storms producing less rainfall but cooler cloud-top temperatures over the Congo. This is in line with conclusions in Hamada et al. (2015) that demonstrate a disconnect between extreme convection and extreme rainfall. Furthermore, an increase in vertical extent of tropical convection is a likely outcome of changes to the Hadley circulation in warmer climates, as reviewed by Fu (2015).

Distinct increases in convective activity over the Angolan Highlands and at the southern tropical edge have been observed (Figs. 11c,d), which corroborates the 2000–16 increase in groundwater storage associated with rainfall increase in this region (Rodell et al. 2018). Little change has been observed over Malawi/Mozambique, southern Tanzania, and Madagascar, which is not surprising since these regions have very large interannual variability, which would increase the signal-to-noise ratio, thereby hindering detection of change (Figs. 11e–g).

North African hotspot convective activity has also increased notably during boreal summer. This increase is reflected over the Ethiopian Highlands (Fig. 11h) and even more prominently over Guinea from May to October (Fig. 11i).

These increases in convective activity in some seasons at these hotspots are reflected in a general increase in annual mean convective activity (Fig. 12; a low-pass filter has been used to exclude interannual variability in the signal). Over west equatorial Africa there has been a 10% increase in widespread convection, computed relative to climatology (Fig. 12a). These trends are even stronger when considering a ccratio computed from CCD_{60} data, both pan-African and for the hotspots (see Figs. S1 and S2 in the online supplemental material). This is in agreement with the trends considered specifically for April–June of the Congo (Raghavendra et al. 2018) and the Sahel wet season of June–September (Taylor et al. 2017).

Notably, the two hotspots with the highest interannual variability, over southern Malawi/Mozambique

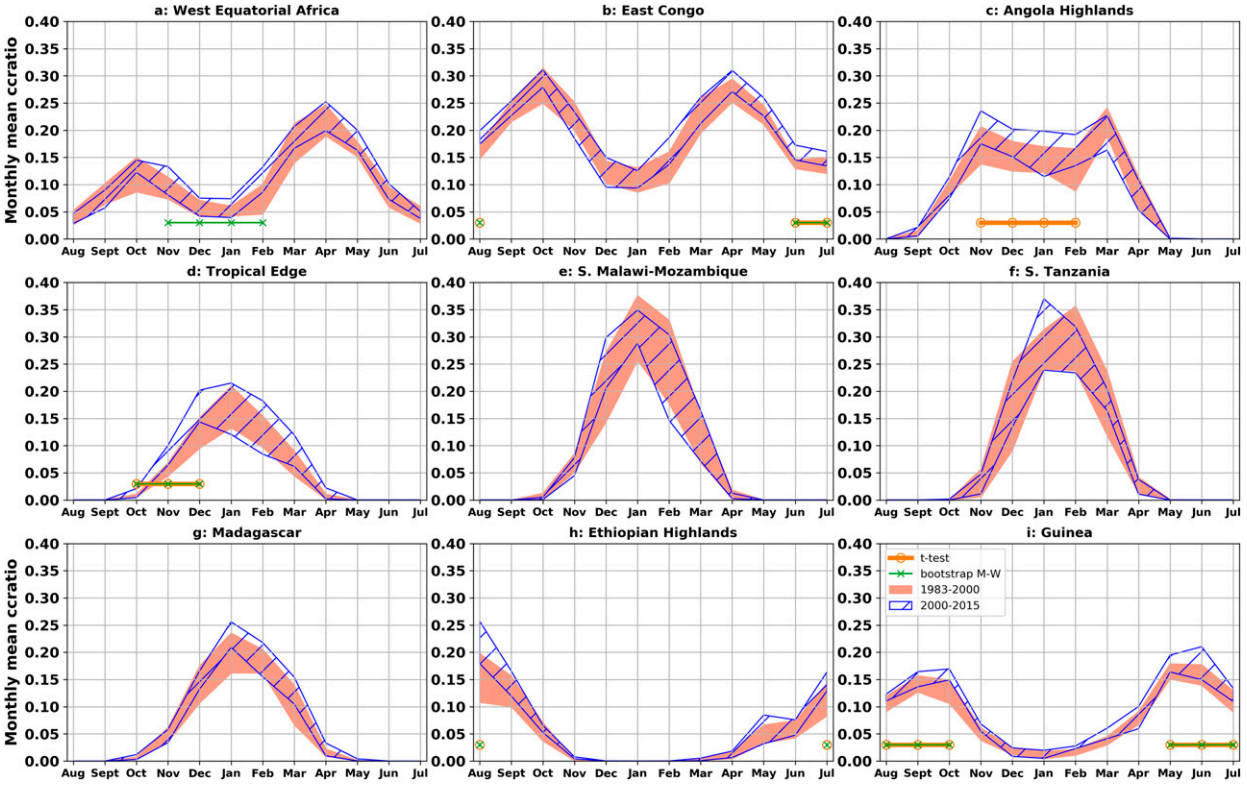

FIG. 11. Contemporary change in the annual cycle of area-averaged convective coverage ratio for the convection hotspots of the African rain belt (see Fig. 8). The interquartile range of monthly mean convective coverage is shown by the width of the curves for seasons that occurred during 1983–2000 (coral shading) and 2000–15 (blue hatching). Months in which the two periods have less than a 5% chance of being drawn from the same distribution are determined by a bootstrapped Mann–Whitney *U* rank test (green line). Significance is additionally considered with a *t* test (orange line).

and southern Tanzania, show wide variations in annual mean convection even on the decadal time scales considered here (Figs. 12e,f). The large noise in the signal in these locations means that negligible long-term change is observed.

The most profound increases are observed along the southern African tropical edge and the Ethiopian Highlands (Figs. 12d and 12h, respectively), with nearly a third more convection in the 2000s relative to the 1980s. This suggests implications for African easterly wave initiation (Mekonnen and Rossow 2011). Indeed, Raghavendra et al. (2019) report increases in activity of the higher-frequency tropical wave activity across the tropics, with the equatorial Rossby wave activity notably increasing downstream (westward) of the Ethiopian Highlands. Patterns in outgoing longwave radiation (OLR) over these highlands suggest a northwestward shift in the location of most intense convection (Raghavendra et al. 2019). However, change convective activity is only part of the total change OLR budget and therefore OLR may be a poor proxy for *changes* in convective activity.

The Angolan Highlands and Guinea hotspot have seen more modest increases of about 20%. We note that all of these increases track the disproportionate warming of the Northern Hemisphere relative to the Southern Hemisphere (gray dashed curves in each panel of Fig. 12) during the satellite observation era. This intriguing correspondence is in keeping with results of Taylor et al. (2017) related to the warming of the Sahara, but also suggests that mechanisms of interhemispheric energy exchange may be at play (Todd and Washington 2004). Further investigation is needed and should build on the work on surface energy balance changes (Zhou et al. 2016; Zhou 2016).

These increases in monthly mean convective activity can be disaggregated into changes in number of convective episodes and the areal extent of these episodes (Fig. 13). Note, however, that increases in intensity (not explicitly considered in this study) would have some impact on areal extent as larger areas of cloud would fall below the −50°C threshold.

Most of the hotspots have had increases in the number of convective objects observed annually with wider

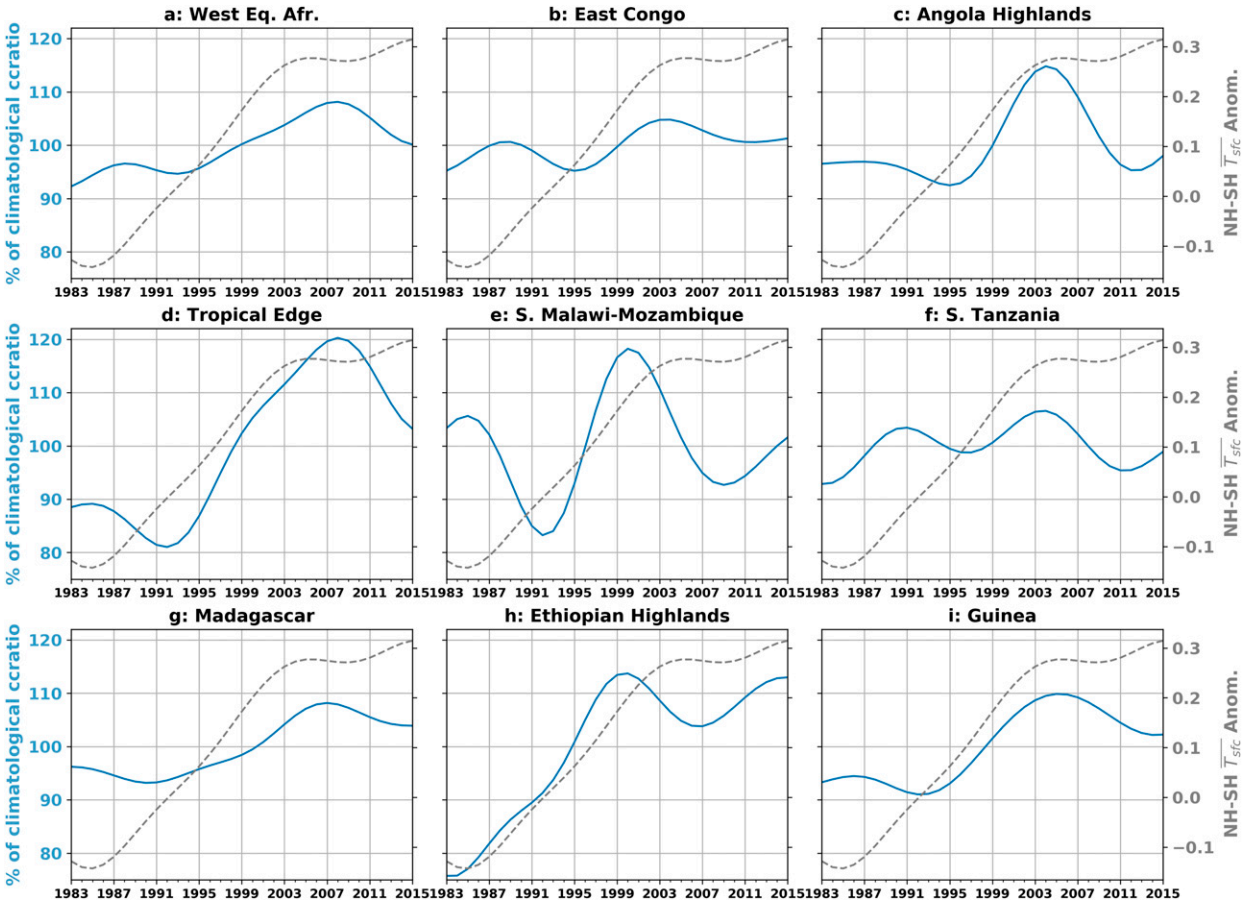

FIG. 12. Low-frequency variation in the annual mean widespread convective activity (percentage of the long-term mean) for convection hotspots (see Fig. 8), as diagnosed from a low-pass (>6 yr) Butterworth filter applied to the satellite-era record (blue line). The low-pass-filtered hemispheric surface temperature difference for the same period is shown for reference (gray dashed line).

variability in the mean areal extent of these convective objects (Fig. 13). Increases in activity in western equatorial Africa, the Angolan Highlands, the southern tropical edge, Madagascar, and Guinea seem all to be a result of general increase in the frequency and areal extent of convection (Fig. 13). However, increases over the Ethiopian Highlands are dominated by the growing size of convective objects (Fig. 13h). Both Malawi/Mozambique and southern Tanzania are dominated by large slow-varying changes in areal extent of convective episodes, further highlighting the large variability inherent over this part of Africa (Figs. 13e,f).

6. Summary

a. The annual cycle

Pan-African convective activity peaks in March, reflecting the vigorous and widespread outbreaks of convection across central and eastern southern Africa. Furthermore, our results have demonstrated that the most widespread and geographically coherent African convection occurs in the transition-season months of October and March/April. This result suggests that energy inputs into the general circulation by African convection may be greatest in the transition seasons.

At a more regional scale, the seasonal march of convective activity in the rain belt is meridionally asymmetric. This is especially true in southern Africa where convection advances primarily down the western half of the continent during October before becoming active in the east during January. This convective activity then retreats from the southeast back into the Congo before the West African monsoon begins. This seasonality of convection is further modulated by regional orographic features with the Angolan Highlands, Virunga/Rwenzori Mountains, Mount Cameroon, and the Ethiopian Highlands all enhancing convective activity and extending the convective seasons relative to their surrounds.

The relatively low-lying plains and hills of southern Malawi, Mozambique, and Tanzania host the most

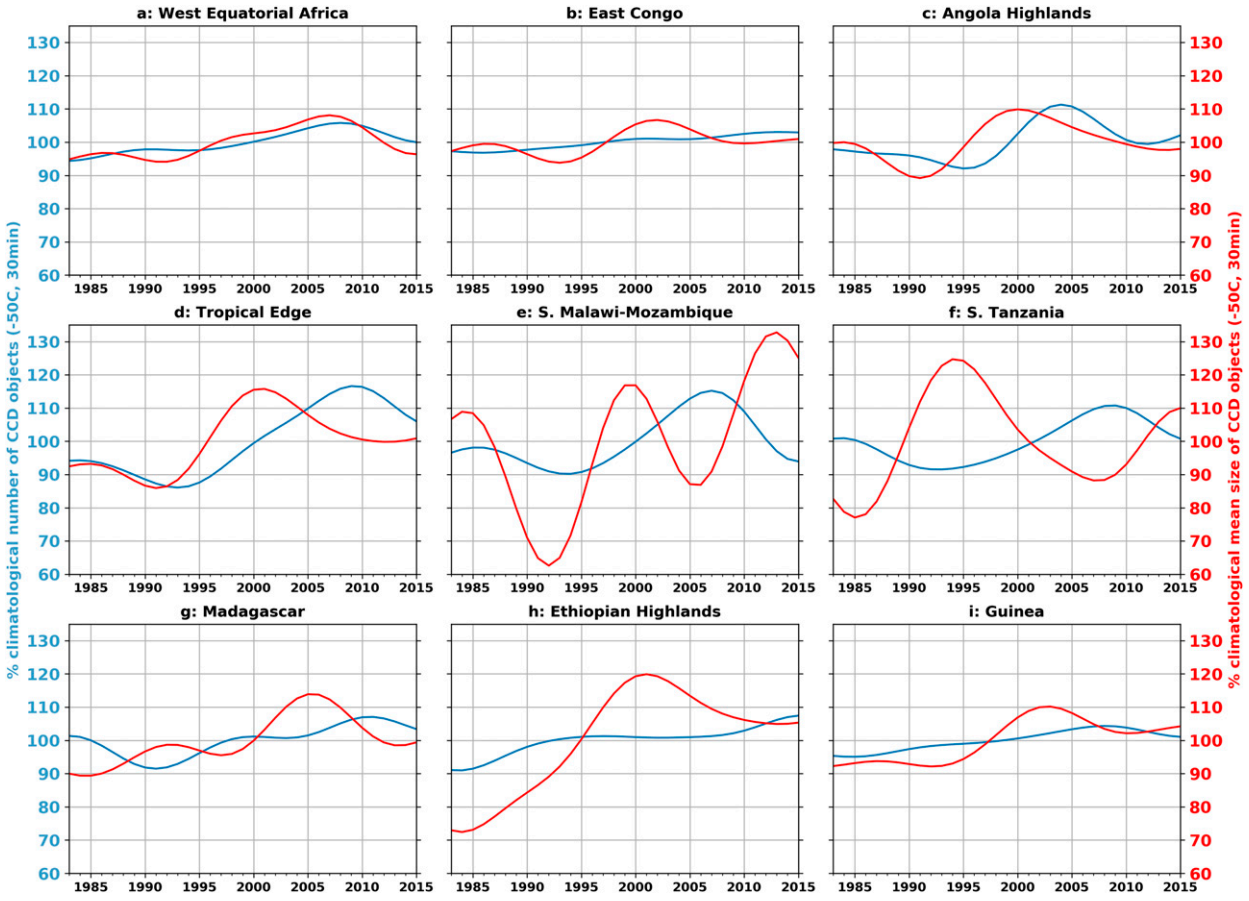

FIG. 13. Separation of ccratio trends presented in Fig. 12 into frequency vs spatial extent of convective activity. Annual mean total number of CCD convective objects (blue line) and the mean areal extent of objects (red line), represented by the percentage of the long-term mean, for convection hotspots (see Fig. 8). Each time series has been smoothed with a low-pass (>6 yr) Butterworth filter to highlight long-term variability.

vigorous convective hotspot of January and February. As highlighted next, this hotspot—with high MSE maintained by convergence of moisture off the Indian Ocean—is the most variable region for widespread convective activity anywhere on the continent.

b. *ENSO-related interannual variability*

The strongest ENSO impacts are during the southern African summer and can be understood as an enhanced southward excursion of the convective activity during La Niña and more equatorward contraction during El Niño. This is in keeping with Nicholson (1986), who reported a mode of African rainfall variability in which the tropics and subtropics demonstrated anomalies of opposite sign. This mode is linked to interannual variability associated with ENSO (Nicholson and Kim 1997). The result is that countries along the southern tropical edge are particularly affected by positive and negative ENSO events. A similar yet muted response to ENSO is observed along the northern edge of the rain belt in North Africa.

The largest ENSO responses are observed in the occurrence of widespread convective outbreaks in eastern southern Africa. The hotspots in convection over southern Malawi/Mozambique and southern Tanzania have the highest observed variability of all the convective hotspots across the continent. These two regions straddle a climate boundary in East Africa, which is seen clearly as the fulcrum of the regional ENSO response: El Niño typically enhances widespread convection over Tanzania and reduces it over southern Malawi and northern Mozambique. La Niña typically enhances convection south of the fulcrum, at the expense of widespread convection to the north over Tanzania. However, these signals are discontinuous through the core summer months, illuminating an intraseasonal complexity that is lost in the typical seasonal mean anomalies.

These regional climates that straddle such a sharp climate boundary are inherently prone to high variability as relatively small shifts in where this boundary is

located year to year can result in large interannual departures in convective rainfall. The likely diversity in the simulated location of such a boundary by different climate models would require careful treatment in regional climate information provision.

c. *Contemporary changes*

There has been a distinct increase, during the satellite era, in pan-African widespread convection with changes in widespread convection of 10%–20% of the climatology observed across deep convective hotspots. This broadly corresponds to a pan-African increase in rainfall, a mode identified in Nicholson (1986). But as shown in recent work on Congo rainfall change, more vigorous convection diagnosed by colder cloud tops may in fact be associated with less rainfall in the tropics (Zhou et al. 2014; Hamada et al. 2015; Raghavendra et al. 2018). However, in regions at the tropical edge of the rain belt such as the Angolan Highlands, more convection does appear to be associated with more rainfall and increased groundwater recharge rates (e.g., Rodell et al. 2018). Similar increases have been observed for most of the hotspots for convection across the continent. These results complement work on rainfall changes in the African monsoon systems [for a review, see Cook and Vizy (2019)].

Statistically distinct changes vary by season across the continent. However, the annual mean changes in convective activity are remarkably consistent with the larger contemporary increase in mean surface temperature of the Northern Hemisphere relative to the Southern Hemisphere. This result is consistent with work over West Africa, which has demonstrated the influence of a warming Sahara on severe precipitation in the most intense MCS systems (Taylor et al. 2017, 2018). This study complements these findings by showing that the hemispheric asymmetry in surface warming is concomitant with pan-African increases the *mean* climatology of widespread convection too.

7. Conclusions

This study set out to develop an integrated picture of widespread convection over the African continent. This approach has allowed important and long overdue results to surface. The first result is the recognition that Africa is most convectively active, in a continental sense, during March. This is primarily a result of frequent widespread outbreaks in both the East Congo and west equatorial Africa. A secondary peak in pan-African convection is observed in October. Together, these results imply that the tropical forcing of the general circulation by African convection may be greatest in the transition seasons (Silva Dias et al. 1983).

The second result to emerge from this continent-wide study is that southeastern Africa hosts the strongest and largest off-equatorial convective hotspot. This region, including Madagascar, is most active during December–February. Such a large off-equatorial heating hotspot is likely to provide an important forcing to extratropical circulation in the Indo-Australian sector of the Southern Hemisphere (Sardeshmukh and Hoskins 1988).

Widespread convection in this southeastern African hotspot also exhibits the largest interannual variability of anywhere on the continent. Much of this variability is related to the influence of ENSO, both due to proximity and the maxima in ENSO anomalies in the Pacific being synchronous with peak convective here.

Throughout the continent the well-documented influence of ENSO is detected in convective activity. In particular, convective hotspots at the edges of core tropical rain belt are prone to less widespread convection during El Niño and more convection during La Niña. This response is reflected in the pan-African mean response, which shows less convective activity across Africa during El Niño.

Finally, this continental-wide study has provided an integration of contemporary changes in convection that have been reported across Africa. Previous studies have focused on convective extremes in particular regions (e.g., Taylor et al. 2017; Raghavendra et al. 2018) or derived rainfall products (e.g., Maidment et al. 2015). We have shown that general increases in *mean* convective activity are observed everywhere. These increases of 10%–20% in annual mean widespread convection across the continent have closely matched the growing interhemispheric asymmetry in warming. This intriguing result warrants speculation that African convection may be more broadly sensitive to interhemispheric energy balances, rather than just warming of the Sahara.

Reconciling the observed annual cycle, variability, and change of deep convection with climate model simulations and projections over Africa is crucial to current efforts at regionalizing global change. The inability of climate simulations to correctly locate Congo rainfall (Creese and Washington 2016, 2018), in contrast to high-confidence results of change in rainfall onset and season length (Dunning et al. 2018), needs careful attention in order to inform climate information needs. And while African convection and rainfall do respond to global forcing, the convective hotspots here identified have the potential to provide a first-order forcing on regional circulation. Whether convection-parameterized general circulation models

represent these local convective forcings needs to be answered. Is this a role best filled by convective-permitting models?

Acknowledgments. This work was carried out under the Future Climate for Africa UMFULA project, with financial support from the U.K. Natural Environment Research Council (NERC), NE/M020207/1 (NCGH and RW), and the U.K. Government's Department for International Development (DfID). The authors particularly thank the UMFULA researchers for valuable conversations and suggestions. Two anonymous reviewers and Ajay Raghavendra are thanked for helping to improve the clarity and presentation of this manuscript.

REFERENCES

Awange, J. L., V. G. Ferreira, E. Forootan, Khandu, S. A. Andam-Akorful, N. O. Agutu, and X. F. He, 2016: Uncertainties in remotely sensed precipitation data over Africa. *Int. J. Climatol.*, **36**, 303–323, https://doi.org/10.1002/joc.4346.

Bjerknes, J., 1969: Atmospheric teleconnections from the equatorial Pacific. *Mon. Wea. Rev.*, **97**, 163–172, https://doi.org/10.1175/1520-0493(1969)097<0163:ATFTEP>2.3.CO;2.

Blamey, R. C., and C. J. C. Reason, 2012: Mesoscale convective complexes over southern Africa. *J. Climate*, **25**, 753–766, https://doi.org/10.1175/JCLI-D-10-05013.1.

Carvalho, L. M. V., and C. Jones, 2001: A satellite method to identify structural properties of mesoscale convection systems based on the maximum spatial correlation technique (MASCOTTE). *J. Appl. Meteor.*, **40**, 1683–1701, https://doi.org/10.1175/1520-0450(2001)040<1683:ASMTIS>2.0.CO;2.

Cook, K. H., and E. K. Vizy, 2019: Contemporary climate change of the African monsoon systems. *Curr. Climate Change Rep.*, **5**, 145–159, https://doi.org/10.1007/s40641-019-00130-1.

Creese, A., and R. Washington, 2016: Using qflux to constrain modeled Congo Basin rainfall in the CMIP5 ensemble. *J. Geophys. Res.*, **121**, 13 415–13 442, https://doi.org/10.1002/2016JD025596.

——, and ——, 2018: A process-based assessment of CMIP5 rainfall in the Congo basin: The September–November rainy season. *J. Climate*, **31**, 7417–7439, https://doi.org/10.1175/JCLI-D-17-0818.1.

Dunning, C. M., E. C. L. Black, and R. P. Allan, 2016: The onset and cessation of seasonal rainfall over Africa. *J. Geophys. Res.*, **121**, 11 405–11 424, https://doi.org/10.1002/2016JD025428.

——, ——, and ——, 2018: Later wet seasons with more intense rainfall over Africa under future climate change. *J. Climate*, **31**, 9719–9738, https://doi.org/10.1175/JCLI-D-18-0102.1.

Fiolleau, T., and R. Roca, 2013: Composite life cycle of tropical mesoscale convective systems from geostationary and low Earth orbit satellite observations: Method and sampling considerations. *Quart. J. Roy. Meteor. Soc.*, **139**, 941–953, https://doi.org/10.1002/qj.2174.

Fu, R., 2015: Global warming-accelerated drying in the tropics. *Proc. Natl. Acad. Sci. USA*, **112**, 3593–3594, https://doi.org/10.1073/pnas.1503231112.

Hamada, A., Y. N. Takayabu, C. Liu, and E. J. Zipser, 2015: Weak linkage between the heaviest rainfall and tallest storms. *Nat. Commun.*, **6**, 6213, https://doi.org/10.1038/ncomms7213.

Hart, N. C. G., C. J. C. Reason, and N. Fauchereau, 2013: Cloud bands over southern Africa: Seasonality, contribution to rainfall variability and modulation by the MJO. *Climate Dyn.*, **41**, 1199–1212, https://doi.org/10.1007/s00382-012-1589-4.

Hartmann, D. L., H. H. Hendon, and R. A. Houze, 1984: Some implications of the mesoscale circulations in tropical cloud clusters for large-scale dynamics and climate. *J. Atmos. Sci.*, **41**, 113–121, https://doi.org/10.1175/1520-0469(1984)041<0113:SIOTMC>2.0.CO;2.

Hodges, K. I., and C. D. Thorncroft, 1997: Distribution and statistics of African mesoscale convective weather systems based on ISCCP Meteosat imagery. *Mon. Wea. Rev.*, **125**, 2821–2837, https://doi.org/10.1175/1520-0493(1997)125<2821:DASOAM>2.0.CO;2.

Houze, R. A., 1982: Cloud clusters and large-scale vertical motions in the tropics. *J. Meteor. Soc. Japan*, **60**, 396–410, https://doi.org/10.2151/jmsj1965.60.1_396.

——, 2004: Mesoscale convective systems. *Rev. Geophys.*, **42**, RG4003, https://doi.org/10.1029/2004RG000150.

Howard, E., and R. Washington, 2018: Characterizing the synoptic expression of the Angola low. *J. Climate*, **31**, 7147–7165, https://doi.org/10.1175/JCLI-D-18-0017.1.

Hua, W., L. Zhou, S. E. Nicholson, H. Chen, and M. Qin, 2019: Assessing reanalysis data for understanding rainfall climatology and variability over central equatorial Africa. *Climate Dyn.*, **53**, 651–669, https://doi.org/10.1007/s00382-018-04604-0.

Jackson, B., S. E. Nicholson, and D. Klotter, 2009: Mesoscale convective systems over western equatorial Africa and their relationship to large-scale circulation. *Mon. Wea. Rev.*, **137**, 1272–1294, https://doi.org/10.1175/2008MWR2525.1.

Kanamitsu, M., W. Ebisuzaki, J. Woollen, S. K. Yang, J. Hnilo, M. Fiorino, and G. L. Potter, 2002: NCEP–DOE AMIP II reanalysis (R-2). *Bull. Amer. Meteor. Soc.*, **83**, 1631–1643, https://doi.org/10.1175/BAMS-83-11-1631.

Knapp, K. R., 2008: Scientific data stewardship of International Satellite Cloud Climatology Project B1 global geostationary observations. *J. Appl. Remote Sens.*, **2**, 023548, https://doi.org/10.1117/1.3043461.

Laing, A. G., R. E. Carbone, and V. Levizzani, 2011: Cycles and propagation of deep convection over equatorial Africa. *Mon. Wea. Rev.*, **139**, 2832–2853, https://doi.org/10.1175/2011MWR3500.1.

Lindesay, J. A., 1988: South African rainfall, the Southern Oscillation and a Southern Hemisphere semi-annual cycle. *Int. J. Climatol.*, **8**, 17–30, https://doi.org/10.1002/joc.3370080103.

Maidment, R. I., D. Grimes, R. P. Allan, E. Tarnavsky, M. Stringer, T. Hewison, R. Roebeling, and E. Black, 2014: The 30 year TAMSAT African rainfall climatology and time series (TARCAT) data set. *J. Geophys. Res.*, **119**, 10 619–10 644, https://doi.org/10.1002/2014JD021927.

——, R. P. Allan, and E. Black, 2015: Recent observed and simulated changes in precipitation over Africa. *Geophys. Res. Lett.*, **42**, 8155–8164, https://doi.org/10.1002/2015GL065765.

——, and Coauthors, 2017: A new, long-term daily satellite-based rainfall dataset for operational monitoring in Africa. *Sci. Data*, **4**, 170063, https://doi.org/10.1038/sdata.2017.63.

Mavume, A. F., L. Rydberg, M. Rouault, and J. R. E. Lutjeharms, 2009: Climatology and landfall of tropical cyclones in the south-west Indian Ocean. *W. Ind. Ocean J. Mar. Sci*, **8**, 15–36, https://doi.org/10.4314/wiojms.v8i1.56672.

Mekonnen, A., and W. B. Rossow, 2011: The interaction between deep convection and easterly waves over tropical North Africa: A weather state perspective. *J. Climate*, **24**, 4276–4294, https://doi.org/10.1175/2011JCLI3900.1.

Neelin, J. D., and I. M. Held, 1987: Modeling tropical convergence based on the moist static energy budget. *Mon. Wea. Rev.*, **115**, 3–12, https://doi.org/10.1175/1520-0493(1987)115<0003:MTCBOT>2.0.CO;2.

Nicholson, S. E., 1986: The spatial coherence of African rainfall anomalies: Interhemispheric teleconnections. *J. Climate Appl. Meteor.*, **25**, 1365–1381, https://doi.org/10.1175/1520-0450(1986)025<1365:TSCOAR>2.0.CO;2.

——, 2018: The ITCZ and the seasonal cycle over equatorial Africa. *Bull. Amer. Meteor. Soc.*, **99**, 337–348, https://doi.org/10.1175/BAMS-D-16-0287.1.

——, and J. Kim, 1997: The relationship of the El Niño–Southern Oscillation to African rainfall. *Int. J. Climatol.*, **17**, 117–135, https://doi.org/10.1002/(SICI)1097-0088(199702)17:2<117::AID-JOC84>3.0.CO;2-O.

——, D. Klotter, A. K. Dezfuli, and L. Zhou, 2018: New rainfall datasets for the Congo Basin and surrounding regions. *J. Hydrometeor.*, **19**, 1379–1396, https://doi.org/10.1175/JHM-D-18-0015.1.

Nie, J., W. R. Boos, and Z. Kuang, 2010: Observational evaluation of a convective quasi-equilibrium view of monsoons. *J. Climate*, **23**, 4416–4428, https://doi.org/10.1175/2010JCLI3505.1.

Ogallo, L. J., 1988: Relationships between seasonal rainfall in East Africa and the Southern Oscillation. *J. Climatol.*, **8**, 31–43, https://doi.org/10.1002/joc.3370080104.

Raghavendra, A., L. Zhou, Y. Jiang, and W. Hua, 2018: Increasing extent and intensity of thunderstorms observed over the Congo Basin from 1982 to 2016. *Atmos. Res.*, **213**, 17–26, https://doi.org/10.1016/j.atmosres.2018.05.028.

——, P. E. Roundy, and L. Zhou, 2019: Trends in tropical wave activity from the 1980s to 2016. *J. Climate*, **32**, 1661–1676, https://doi.org/10.1175/JCLI-D-18-0225.1.

Rapolaki, R. S., and C. J. C. Reason, 2018: Tropical storm Chedza and associated floods over south-eastern Africa. *Nat. Hazards*, **93**, 189–217, https://doi.org/10.1007/s11069-018-3295-y.

Rasmusson, E. M., and T. H. Carpenter, 1982: Variations in tropical sea surface temperature and surface wind fields associated with the Southern Oscillation/El Niño. *Mon. Wea. Rev.*, **110**, 354–384, https://doi.org/10.1175/1520-0493(1982)110<0354:VITSST>2.0.CO;2.

Reason, C. J. C., W. Landman, and W. Tennant, 2006: Seasonal to decadal prediction of southern African climate and its links with variability of the Atlantic Ocean. *Bull. Amer. Meteor. Soc.*, **87**, 941–955, https://doi.org/10.1175/BAMS-87-7-941.

Reynolds, R. W., N. A. Rayner, T. M. Smith, D. C. Stokes, and W. Wang, 2002: An improved in situ and satellite SST analysis. *13th Symp. on Global Change and Climate Variations*, Orlando, FL, Amer. Meteor. Soc., 8.2., https://ams.confex.com/ams/annual2002/webprogram/Paper26750.html.

Roca, R., and Coauthors, 2010: On the water and energy cycles in the tropics. *C. R. Geosci.*, **342**, 390–402, https://doi.org/10.1016/j.crte.2010.01.003.

——, J. Aublanc, P. Chambon, T. Fiolleau, and N. Viltard, 2014: Robust observational quantification of the contribution of mesoscale convective systems to rainfall in the tropics. *J. Climate*, **27**, 4952–4958, https://doi.org/10.1175/JCLI-D-13-00628.1.

Rodell, M., J. S. Famiglietti, D. N. Wiese, J. T. Reager, H. K. Beaudoing, F. W. Landerer, and M.-H. Lo, 2018: Emerging trends in global freshwater availability. *Nature*, **557**, 651–659, https://doi.org/10.1038/s41586-018-0123-1.

Rodwell, M. J., and Coauthors, 2013: Characteristics of occasional poor medium-range weather forecasts for Europe. *Bull. Amer. Meteor. Soc.*, **94**, 1393–1405, https://doi.org/10.1175/BAMS-D-12-00099.1.

Sardeshmukh, P. D., and B. J. Hoskins, 1988: The generation of global rotational flow by steady idealized tropical divergence. *J. Atmos. Sci.*, **45**, 1228–1251, https://doi.org/10.1175/1520-0469(1988)045<1228:TGOGRF>2.0.CO;2.

Silva Dias, P. L., W. H. Schubert, and M. DeMaria, 1983: Large-scale response of the tropical atmosphere to transient convection. *Atmos. Sci.*, **40**, 2689–2707, https://doi.org/10.1175/1520-0469(1983)040<2689:LSROTT>2.0.CO;2.

Stratton, R. A., and Coauthors, 2018: A pan-African convection-permitting regional climate simulation with the Met Office Unified Model: CP4-Africa. *J. Climate*, **31**, 3485–3508, https://doi.org/10.1175/JCLI-D-17-0503.1.

Taylor, C. M., and Coauthors, 2017: Frequency of extreme Sahelian storms tripled since 1982 in satellite observations. *Nature*, **544**, 475–478, https://doi.org/10.1038/nature22069.

——, A. H. Fink, C. Klein, D. J. Parker, F. Guichard, P. P. Harris, and K. R. Knapp, 2018: Earlier seasonal onset of intense mesoscale convective systems in the Congo Basin since 1999. *Geophys. Res. Lett.*, **45**, 13 458–13 467, https://doi.org/10.1029/2018GL080516.

Todd, M. C., and R. Washington, 2004: Climate variability in central equatorial Africa: Influence from the Atlantic sector. *Geophys. Res. Lett.*, **31**, L23202, https://doi.org/10.1029/2004GL020975.

van der Walt, S., and Coauthors, 2014: scikit-image: Image processing in Python. *PeerJ*, **2**, e453, https://doi.org/10.7717/peerj.453.

Ventura, V., C. J. Paciorek, and J. S. Risbey, 2004: Controlling the proportion of falsely rejected hypotheses when conducting multiple tests with climatological data. *J. Climate*, **17**, 4343–4356, https://doi.org/10.1175/3199.1.

Waliser, D. E., and C. Gautier, 1993: A satellite-derived climatology of the ITCZ. *J. Climate*, **6**, 2162–2174, https://doi.org/10.1175/1520-0442(1993)006<2162:ASDCOT>2.0.CO;2.

Ward, M. N., 1992: Provisionally corrected surface wind data, worldwide ocean–atmosphere surface fields, and Sahelian rainfall variability. *J. Climate*, **5**, 454–475, https://doi.org/10.1175/1520-0442(1992)005<0454:PCSWDW>2.0.CO;2.

Washington, R., R. James, H. Pearce, W. M. Pokam, and W. Moufouma-Okia, 2013: Congo basin rainfall climatology: Can we believe the climate models? *Philos. Trans. Roy. Soc.*, **368B**, 20120296, https://doi.org/10.1098/rstb.2012.0296.

Webster, P. J., 1973: Temporal variation of low-latitude zonal circulations. *Mon. Wea. Rev.*, **101**, 803–816, https://doi.org/10.1175/1520-0493(1973)101<0803:TVOLZC>2.3.CO;2.

Zhou, L., 2016: Desert amplification in a warming climate. *Sci. Rep.*, **6**, 31065, https://doi.org/10.1038/srep31065.

——, and Coauthors, 2014: Widespread decline of Congo rainforest greenness in the past decade. *Nature*, **509**, 86–90, https://doi.org/10.1038/nature13265.

——, H. Chen, W. Hua, Y. Dai, and N. Wei, 2016: Mechanisms for stronger warming over drier ecoregions observed since 1979. *Climate Dyn.*, **47**, 2955–2974, https://doi.org/10.1007/s00382-016-3007-9.